

**Cu-Au type orderings in the staggered quadrupolar region of the  
fcc Blume Emery Griffiths model**

Aycan Özkan<sup>1</sup>, Bülent Kutlu<sup>2</sup>

<sup>1</sup>Gazi Üniversitesi, Fen Bilimleri Enstitüsü, Fizik Anabilim Dalı, Ankara,  
Turkey

<sup>2</sup>Gazi Üniversitesi, Fen -Edebiyat Fakültesi, Fizik Bölümü, 06500  
Teknikokullar, Ankara, Turkey

E-mail: aycan@gazi.edu.tr and bkutlu@gazi.edu.tr

The spin-1 Ising (BEG) model has been simulated using a cellular automaton (CA) algorithm improved from the Creutz cellular automaton (CCA) for a face-centered cubic (fcc) lattice. The ground state diagram ( $k$ ,  $d$ ) of the fcc BEG model has ferromagnetic ( $F$ ), quadrupolar ( $Q$ ) and staggered quadrupolar ( $SQ$ ) ordering regions. The simulations have been made in the staggered quadrupolar region for the parameter values in the intervals  $-24 \leq d = D/J < 0$  and  $-3 \leq k = K/J \leq 0$ . The phase diagrams on the  $(kT_C/J, d)$  and the  $(kT_C/J, k)$  planes have been obtained through  $k = -3$  and  $d = -4$  lines, respectively. The staggered quadrupolar ordering region separates into five ordering regions ( $A_3B(a)$ ,  $A_3B(f)$ ,  $AB$  (type-I),  $AB$  (type-II) and  $AB_3(f)$ ) which have the different stoichiometric Cu-Au type structures.

Key words: Spin-1 Ising (BEG) model; Cellular automaton; phase diagram; face-centered-cubic lattice

### 1 . Introduction

The Blume-Emery-Griffiths (BEG) model [1] is a spin-1 Ising model with

very rich and interesting phase structure. Some of models in the statistical mechanics can be regarded as special cases of a general Ising model. The lattice gas Hamiltonian may be written in terms of site occupation operators  $P_i^\lambda$  constituting by the Ising spin energy [2 – 12]. In this case, the generalized Hamiltonian is defined as [6, 13]

$$H = \sum_{\lambda, \nu} \sum_{i, j} I_{ij}^{\lambda\nu} P_i^\lambda P_j^\nu + \sum_{\lambda} \sum_i V_i^\lambda P_i^\lambda + H_0 \quad (1)$$

where the  $I_{ij}^{\lambda\nu}$  describes the interaction between species  $\lambda$  and  $\nu$  on sites  $i$  and  $j$ , respectively. Second term in Eq. (1) describes the binding energy. The irrelevant terms are included in  $H_0$ . If site  $i$  is occupied by species  $\lambda$ ,  $P_i^\lambda$  is equal to 1, and zero otherwise. This energy definition is also valid for the ternary alloys [6]. This model can be related to spin-1 Ising model by the following transformations:

$$P_i^A = S_i(S_i - 1)/2$$

$$P_i^B = S_i(S_i + 1)/2$$

$$P_i^C = 1 - S_i^2$$

The three components of the spin variables  $S_i$  are related with each species of atoms:  $S_i = -1$  (A),  $+1$  (B) and  $0$  (C) for the  $((AB)_{1-x}C_{2x})$  ternary alloys or  $S_i = 0$  ( $Cu$ ) and  $\pm 1$  ( $Au$ ) for  $Cu$ - $Au$  type alloys. The Hamiltonian is then equivalent to the spin-1 Ising Hamiltonian

$$H_I = -J \sum_{\langle ij \rangle} S_i S_j - K \sum_{\langle ij \rangle} S_i^2 S_j^2 + L \sum_{\langle ij \rangle} (S_i S_j^2 + S_i^2 S_j) + D \sum_i S_i^2 + h \sum_i S_i + H'_0 \quad (2)$$

where

$$J = -(J_{AA} + J_{BB})/4 - J_{AB}/2 \quad (3)$$

$$K = -(J_{AA} + J_{BB})/4 + J_{AB}/2 - J_{AC} - J_{BC} + J_{CC} \quad (4)$$

$$L = (J_{AA} - J_{BB})/4 + (J_{AC} - J_{BC})/2 \quad (5)$$

$$D = z(2J_{CC} - J_{BC} - J_{AC}) - V_B - V_A + 2V_C \quad (6)$$

$$h = z(J_{BC} - J_{AC}) + V_B - V_A \quad (7)$$

$J, K, L, D, h$  and  $H_0^l$  are bilinear, biquadratic, dipol-quadrupol interaction terms, single-ion anisotropy constant, the field term and irrelevant terms, respectively.  $\langle ij \rangle$  denotes summation over all nearest-neighbor ( $nn$ ) pairs of sites.

The spin-1 Ising (BEG) model was firstly studied to determine the phase separation and superfluid ordering in He<sup>3</sup>-He<sup>4</sup> mixtures [1]. Variants of the model have been extensively studied because of the fundamental interest in the tricritical, reentrant and multicritical phenomena [14 – 16] of physical systems such as solid-liquid-gas systems [2], the multicomponent fluids [3], the microemulsions [4], the metastable alloys [5, 6, 17] and the binary alloys [18]. The BEG model has been investigated using many different approximate and simulation techniques in the special phase regions for different

lattice type and dimensions. These studies show that the fcc BEG model with repulsive biquadratic coupling has the staggered quadrupolar ( $SQ$ ) ordering phase region in the ( $k = K/J$ ,  $d = D/J$ ) ground state diagram for the  $k < -1$  parameter region [19 – 27], but there are the different results for the phase boundaries between the  $SQ$  ordering region and the other ordering regions. Furthermore, the  $SQ$  ordering region includes the Cu-Au ( $A_3B$ ,  $AB$  and  $AB_3$ ) type stoichiometric structures as the ground state ordering [24, 25]. The special orders of the Cu-Au ( $A_3B$ ,  $AB$  and  $AB_3$ ) type binary alloys are investigated by the MC [28 – 32], the CVM [33, 34] and the mean field theory [35, 36] considering also the spin-1/2 Ising model, the effective medium theory (EMT) [31, 36], the Bozzola Ferrante Smith (BFS) [32] method and the numerical calculation [37]. The Cu-Au type structures are also studied experimentally by the x-ray diffraction [39 – 42], the nuclear magnetic resonance (NMR) [43], the galvanic cell study [44], the electrical resistivity [45] and the electron diffraction [46, 47] in the binary alloys. Some of the theoretical [31, 36, 37] and the experimental studies [39, 41 – 47] for CuAu type structures have indicated that the  $AB$  ordering structure separated into two different structure as the modulated  $AB$  (type-II) phase and the  $AB$  (type-I) phase. The modulated  $AB$  (type-II) phase is produced from unit cells of the modulated  $AB$  (type-I) phase and is characterized by the existence of antiphase boundaries [46]. In this work, we have been investigated the Cu-Au type structures using an alternative algorithm improved from cellular automaton for the fcc the BEG model with repulsive biquadratic coupling. In the previous papers, the Creutz cellular automaton (CCA) algorithm and

improved versions have been used successfully to study the properties of the critical behaviors of the Ising model Hamiltonians [15, 16, 48 – 67]. The CCA algorithm, which was first introduced by Creutz [53], is a microcanonical algorithm interpolating between the conventional Monte Carlo and the molecular dynamics techniques for Ising model.

The basic aim of this study is to investigate the existence of the modulated  $AB$  (type-II) phase and the critical behavior of the Cu-Au ( $A_3B$ ,  $AB$  and  $AB_3$ ) type stoichiometric structures on the fcc BEG model using the heating algorithm [15, 16] improved from cellular automaton. For this purpose, the fcc BEG model is simulated on a cellular automaton (CA) through the  $k = -3$  and  $d = -4$  lines in the  $-24 \leq d < 0$  and  $-3 \leq k \leq 0$  parameter region, respectively. The temperature variations of the four sublattice order parameters ( $m_a, q_a$ ), the four sublattice susceptibilities ( $\chi_a$ ), the lattice specific heat ( $C/k$ ) and the lattice Ising energy ( $H_I$ ) were computed on the fcc lattice with linear dimension  $L = 9$  for  $J > 0$ ,  $L = 0$  and  $H = 0$ . The finite lattice critical temperatures are estimated from the maxima of the specific heat ( $C/k$ ) and the sublattice susceptibilities ( $\chi_a$ ) to get the phase diagrams. The CA results for the 5% heating rate nearly agree with the CVM and MFA results for the critical lines. In addition, it is seen that the fcc BEG model on the cellular automaton exhibits the modulated  $AB$  (type-II) phase as indicated by the theoretical studies [31, 36, 37] and the experimental results [39, 41 – 47] for Cu-Au type structures.

## 2. Results and discussion

The simulations have been performed on the face-centered cubic lattice

for linear dimension  $L=9$  with periodic boundary conditions using heating algorithm (The total number of sites is  $N = 4L^3$ ). This algorithm is realized by increasing of 5% in the kinetic energy ( $H_k$ ) of each site [15]. Therefore, the increasing value per site of  $H_k$  is obtained from the integer part of the  $0.05H_k$ . In this study, +1 and -1 values of spin variable  $S_i$  are related with species  $B$  (Au), while species  $A$  (Cu) is represented with 0 value of  $S_i$ . The computed values of the thermodynamic quantities are averages over the lattice and over the number of time steps (1.000.000) with discard of the first 100.000 time steps during which the cellular automaton develops.

The ground state diagram of the fcc BEG model is illustrated in Fig. 1. The ground state phase diagram of the fcc BEG model has the ferromagnetic ( $F$ ), the staggered quadrupolar ( $SQ$ ) and the quadrupolar ( $Q$ ) ordering regions on the  $(k, d)$  plane. Furthermore the staggered quadrupolar ordering region separates into three regions which have the  $A_3B$ ,  $AB$  and  $AB_3$  orderings [24]. The initial simulations obtained for some  $d$  and  $k$  parameter values in the interval  $-24 \leq d \leq 0$  through the  $k = -3$  line are shown that the lattice order parameters ( $M, Q$ ) do not have any sign in low temperature region while the behavior of the lattice Ising energy ( $H_I$ ) indicate a phase transition. Therefore, the sublattices have been followed to distinguish the type of the phases and the phase transitions. The temperature dependence of the sublattice order parameters are different each other at the ferrimagnetism and the antiquadrupolar phases [21, 22, 24].

The fcc lattice can be built from the four interpenetrating simple cubic (sc) lattices, called sublattices. The sublattice order parameters ( $m_\alpha, q_\alpha$ ) are

calculated as

$$m_\alpha = |\langle S_i \rangle|_\alpha = \frac{1}{N_\alpha} \left| \sum_{i=1}^{N_\alpha} S_{i\alpha} \right| \quad (8)$$

$$q_\alpha = \langle S_i^2 \rangle_\alpha = \frac{1}{N_\alpha} \sum_{i=1}^{N_\alpha} S_{i\alpha}^2 \quad (9)$$

where  $\alpha$  indicate sublattices ( $\alpha = a, b, c, d$ ) (Fig. 2).

According to the values of the sublattice order parameters, the model has the five different phases ( $P$ ,  $F$ ,  $A_3B(a)$ ,  $AB_3(f)$ ,  $AB$  (type-1)) at absolute zero temperature and two different phases ( $A_3B(f)$  and  $AB$  (type-II)) above absolute zero temperature for  $-3 \leq k < -1$  [21, 24]:

Paramagnetic ( $P$ )  $m_\alpha = 0$  ( $\alpha = a, b, c, d$ ),  $q_a = q_b = q_c = q_d > 0$ ,

Ferromagnetic ( $F$ )  $m_a = m_b = m_c = m_d \neq 0$ ,  $q_a = q_b = q_c = q_d > 0$ ,

Antiquadrupolar  $A_3B(a)$   $m_\alpha = 0$  ( $\alpha = a, b, c, d$ ),  $q_a > q_b = q_c = q_d \geq 0$ ,

Ferrimagnetic  $A_3B(f)$   $m_a > m_b = m_c = m_d > 0$ ,  $q_a > q_b = q_c = q_d > 0$ ,  
( $m_\alpha = q_\alpha$ ,  $\alpha = a, b, c, d$ ),

Ferrimagnetic  $AB_3(f)$   $m_b = m_c = m_d > m_a > 0$ ,  $q_b = q_c = q_d > q_a > 0$ ,  
( $m_\alpha = q_\alpha$ ,  $\alpha = a, b, c, d$ ),

Ferrimagnetic  $AB$  (type-I)  $m_a = m_b = 1$ ,  $m_c = m_d = 0$ ,  $q_a = q_b = 1$ ,  
 $q_c = q_d = 0$ , ( $m_\alpha = q_\alpha$ ,  $\alpha = a, b, c, d$ ).

Ferrimagnetic  $AB$  (type-II)  $m_c = m_d > m_a = m_b > 0$ ,  $q_c = q_d > q_a = q_b > 0$ ,  
( $m_\alpha = q_\alpha$ ,  $\alpha = a, b, c, d$ ).

These phase definitions except  $AB$  ordering structure are compatible with the MFA and the CVM studies [21, 24, 25]. In this study ferrimagnetic  $AB$  ordering structure appears as  $AB$  (type-I) and  $AB$  (type-II) ordering structures while the MFA and the CVM studies do not exhibit this separation. In

the  $AB$  (type-I) ordering structure, two of the sublattices are occupied by  $B$  ( $S_i = +1$  or  $-1$ ) species ( $m_a = m_b = 1, q_a = q_b = 1$ ), while the other sublattices are occupied by  $A$  ( $S_i = 0$ ) species ( $m_c = m_d = 0, q_c = q_d = 0$ ) on the fcc lattice. In the ferrimagnetic  $AB$  (type-II) ordering structure, the  $A$  and  $B$  chains interchange periodically on the fcc lattice. This is a modification of the  $AB$  (type-I) ordering structure [36, 46, 68 – 70].

### 2.1. The phase transitions on the Cu-Au type orderings

The temperature variations of the sublattice order parameters ( $m_\alpha, q_\alpha$ ), the sublattice susceptibility ( $\chi_\alpha$ ), the lattice Ising energy ( $H_I$ ), and the lattice specific heat ( $C/k$ ) are calculated to determine the types of the phase transitions in the interval  $-24 \leq d < 0$  through the  $k = -3$  line and in the interval  $-3 < k < 0$  through the  $d = -4$  line. For producing the phase diagrams, the finite lattice critical temperatures are estimated from the maxima of the specific heat ( $C/k$ ) and the sublattice susceptibilities ( $\chi_\alpha$ ) on the lattice with  $L=9$ .

In the interval  $-8 < d < 0$  through the  $k = -3$  line, the model has the paramagnetic  $A_3B(P)$  ground state ordering. In the  $A_3B(P)$  ordering structure, three of the sublattices are occupied by  $A$  ( $S_i = 0$ ) species ( $m_b = m_c = m_d = 0, q_b = q_c = q_d = 0$ ), while the other sublattice is occupied randomly by  $B$  ( $S_i = +1$  and  $-1$ ) species ( $m_a = 0, q_a = 1$ ). The temperature dependences of the thermodynamic quantities are given in Fig. 3 for representing the  $A_3B(a) - P$  phase transition at a selected ( $d = -4, k = -3$ ) point on the ( $k, d$ ) plane. It can be clearly seen that, as temperature increases, the sublattice order parameter  $q_a$  decreases sharply from unity to a

value ( $\sim 0.25$ ) of the paramagnetic ordering and coincide with  $q_b$ ,  $q_c$  and  $q_d$  at a transition temperature  $kT_t/J$ . Furthermore, the sublattice order parameters ( $m_\alpha(\alpha = a, b, c, d)$ ) do not exhibit any change from initial value. For this transition, the sublattice order parameters  $q_\alpha$  and the Ising energy are in s-shape nature (Fig. 3(a) and 3(c)) while the sublattice susceptibilities and the specific heat show a sharp peak at the transition temperature  $kT_t/J$  (Fig. 3(b) and 3(d)). The  $A_3B(a) - P$  phase transition is of first order for  $d = -4$  and  $k = -3$ . The model has a similar behavior for some  $d$  parameter values in  $-7 \leq d \leq 0$  parameter region through the  $k = -3$  line. However, the phase transition is usually of second order for  $d$  parameter values in this region. On the other hand, the lattice order parameters ( $M, Q$ ) indicate the paramagnetic ordering and they do not show any sign at the  $A_3B(a) - P$  phase transition in this parameter region (Fig. 3(a)). This result shows that the observing of the sublattices is necessary to decide the type of ordering and the phase transition. In the interval  $-7.3 < d < -7$  for  $k = -3$ , the model exhibits the second order successive  $A_3B(a) - F - P$  phase transition. As it is seen in Fig. 4, the sublattice order parameters continuously increase to a value of ferromagnetic  $F$  ordering ( $m_a = m_b = m_c = m_d = 0.20$ ,  $q_b = q_c = q_d = 0.25$ ) from the  $A_3B(a)$  ground state ordering near the critical temperature  $kT_{C1}/J$ . At high temperatures, the  $F$  ordering tends to paramagnetic  $P$  ordering. In this interval, the sublattice order parameters and the lattice Ising energy appear continuous near the critical temperatures  $kT_{C1}/J$  and  $kT_{C2}/J$  while the lattice susceptibility and the sublattice susceptibility and the lattice specific heat have two characteristic peaks at these

temperatures. The all phase transitions are of the second order in this region.

On the  $(k, d)$  plane, the model does not have any ground state ordering between the  $A_3B(a)$  and  $AB$  (type-I) ground state ordering regions. However, the CA results show that there are successive  $A_3B(P) - A_3B(f) - F - P$  phase transitions in the interval  $-8 < d < -7$  through the  $k = -3$  line. The temperature variations of the thermodynamic quantities are illustrated in Fig. 5 for selected  $d = -7.7$  parameter value. For this parameter, the model has  $A_3B(a)$  ground state ordering. With increasing temperature, the  $A_3B(P)$  ordering tends to the ferrimagnetic  $A_3B(f)$  ordering near the critical temperature as CVM result [24]. At a certain temperature above the critical temperature  $kT_{C1}/J$ , the sublattice order parameters coincide ( $m_\alpha = 0.3$ ,  $q_\alpha = 0.35$  ( $\alpha = a, b, c, d$ )) with each other. In this case, the amount of the  $A$  ( $S_i = 0$ ) and the  $B$  ( $S_i = +1$  or  $-1$ ) species on the each sublattices are equal and the ordering of the system changes from  $A_3B(f)$  to  $F$  at the critical temperature  $kT_{C2}/J$ . At a critical temperature  $kT_{C3}/J$  above the critical temperature  $kT_{C2}/J$ , the model exhibits the second order  $F$ - $P$  phase transition. As it is seen in Fig. 5, the sublattice susceptibilities and the lattice specific heat have the three characteristic peaks while the sublattice order parameters and the lattice Ising energy exhibit continuity for the successive phase transitions. This case indicates that the successive  $A_3B(a) - A_3B(f) - F - P$  phase transitions are of the second order.

For the interval  $-16 < d < -8$  through the  $k = -3$  line, the model takes the  $AB$  (type-I) ordering structure as ground state, thus  $m_a = m_b = 1$ ,  $q_a = q_b = 1$ ,  $m_c = m_d = 0$  and  $q_c = q_d = 0$  at  $kT/J = 0$ . In Fig.

6, temperature variations of the thermodynamic quantities are illustrated for the  $d = -12$  value through the  $k = -3$  line. It can be clearly seen that as temperature increases  $m_a = m_b$  and  $q_a = q_b$  decreases sharply from unity to a value of the ferromagnetic ordering and coincide with  $m_c = m_d$  and  $q_c = q_d$  at a certain temperature,  $kT_t/J$ . There are the successive  $AB$  (type-I)– $F$ – $P$  phase transitions. At the  $AB$  (type-I)– $F$  phase transition, the sublattice order parameters and the lattice Ising energy are in s-shape nature at the transition temperature  $kT_t/J$  (Fig. 6(a) and 6(c)) and the sublattice susceptibility and the lattice specific heat have a sharp peak at  $kT_t/J$ . For the  $F$ – $P$  phase transition, the sublattice order parameters and the lattice Ising energy appear continuously near the critical temperature  $kT_C/J$  (Fig. 6(a) and 6(c)). At the same time, the sublattice susceptibility and the lattice specific heat have a characteristic peak at  $kT_C/J$  for this transition (Fig. 6(b) and 6(d)). The results show that the  $AB$  (type-I)– $F$  and the  $F$ – $P$  phase transitions for  $d = -12$  parameter value are of the first order and of the second order, respectively. However, the  $AB$ (type-I)– $F$  phase transition is of the second order for the all values of the  $d$  parameter except  $d = -12$  in the interval  $-15.5 < d < -8$ .

In the intervals  $-15.8 < d < -14$ ,  $-14 < d < -12$ ,  $-12 < d < -10$  and  $-10 < d < -8.3$  of the phase space, the model has the ferrimagnetic  $AB$  (type-II) ordering between ferrimagnetic  $AB$  (type-I) and  $F$  orderings. The  $AB$  (type-II) ordering is determined from the behavior of the sublattice order parameters ( $m_\alpha, q_\alpha$ ) and peaks of the sublattice susceptibilities ( $\chi_\alpha$ ) and the lattice specific heat ( $C/k$ ). For a selected  $d = -14.5$  value, the temper-

ature variations of the thermodynamic quantities are shown in Fig. 7. The temperature dependences of the thermodynamic quantities show that the model exhibits the successive  $AB$  (type-I)– $F$ – $AB$  (type-II)– $F$ – $P$  phase transitions in these intervals. At the low temperature region of the successive phase transition, the sublattice order parameters  $m_a = m_b = q_a = q_b$  decreases from unity to a value ( $\sim 0.58$ ) of the ferromagnetic ordering and coincide with  $m_c = m_d = q_c = q_d$  parameters at the  $kT_{C1}/J$  temperature. This case indicates the phase transition from  $AB$  (type-I) to  $F$  order. At a critical temperature  $kT_{C2}/J$  above the  $kT_{C1}/J$ , the sublattice order parameters change their positions and part equally from  $m_\alpha = q_\alpha \sim 0.58$  to produce the  $AB$  (type-II) ordering. It can be seen from Fig. 7(a) that the model exhibits  $AB$  (type-II) ordering in the certain temperature range. As the temperature increases, the sublattice order parameters coincide again with each other and there occur the  $F$  ordering at the critical temperature  $kT_{C3}/J$  above the critical temperature  $kT_{C2}/J$ . Finally, the sublattice order parameters  $m_\alpha$  decrease to the value ( $m_\alpha \sim 0$ ) of  $P$  ordering near a high temperature  $kT_{C4}/J$  above  $kT_{C3}/J$ . The sublattice order parameters ( $m_a, q_a$ ) and the lattice Ising energy ( $H_I$ ) show continuity (Fig. 7(a) and 7(c)) at the these successive phase transitions while the sublattice susceptibilities ( $\chi_\alpha$ ) exhibit the broad peak with a strong peak at  $kT_{C1}/J$  and a shoulder at  $kT_{C2}/J$ , a weak peak at  $kT_{C3}/J$  and a characteristic peak at  $kT_{C4}/J$  for the  $0.05H_K$  value of the heating rate (Fig. 7(b)). However, the lattice specific heat ( $C/k$ ) have a characteristic peak ( $kT_{C1}/J$ ), a broad peak ( $kT_{C3}/J$  and  $kT_{C2}/J$ ) and a strong peak at high temperature region ( $kT_{C4}/J$ ) (Fig.

7(d)). Therefore, all of the successive  $AB$  (type-I)– $F$ – $AB$  (type-II)– $F$ – $P$  phase transitions are of second order in these parameter regions. The simulations are repeated at the different heating rates and the linear dimensions for checking the existence of the  $AB$  (type-I)– $F$ – $AB$  (type-II) phase transitions at the different  $d$  values. The results of the sublattice susceptibilities and the lattice specific heat for the  $0.01H_K$  and  $0.05H_K$  values of the heating rate are illustrated in Fig. 7(b) and (d). It can be clearly seen from figure that the lattice Ising energy exhibits a critical behavior compatible with the sublattice order parameter at the low temperature region while the broad peaks in the sublattice susceptibilities and the lattice specific heat for  $0.05H_k$  are separate into the three peaks at the simulations with the  $0.01H_K$  heating rate. Consequently, there are a peak corresponding to each phase transitions for the successive  $AB$  (type-I)– $F$ – $AB$  (type-II)– $F$  phase transitions. On the other hand, the calculations for different lattice sizes ( $L = 6, 9$  and  $15$ ) show that the model exhibits the  $AB$  (type-II) phase which occurs independently from linear dimension of lattice.

At phase boundary between the  $AB$  (type-I) and the  $AB_3(f)$  ground state regions, the model exhibits the multi  $AB$  (type-I)– $F$ – $AB$  (type-I)– $F$ – $P$  phase transition. In Fig. 8, the temperature variations of the thermodynamic quantities are shown for  $d = -15.8$  parameter value. The ground state ordering for this parameter value is  $AB$  (type-I). At low temperature region, the sublattice order parameters  $m_a = m_b = q_a = q_b$  decreases sharply from unity to a value ( $\sim 0.6$ ) of ferromagnetic ordering and coincide with the  $m_c = m_d = q_c = q_d$  parameters at a transition temperature  $kT_{t1}/J$ . For the

first order  $AB$  (type-I)– $F$  phase transition, the sublattice order parameters and the lattice Ising energy are in s-shape nature (Fig. 8(a) and 8(c)) while the sublattice susceptibility and the lattice specific heat show a jump at the transition temperature (Fig. 8(b) and 8(d)). At a certain temperature above  $kT_{t1}/J$ , the sublattice order parameters part equally from  $m_\alpha = q_\alpha = 0.6$ . In this case, the model has the  $AB$  (type-I) ordering above a transition temperature  $kT_{t2}/J$ . At this transition, sublattice order parameters and the lattice Ising energy appear discontinuously and sublattice susceptibilities and the lattice specific heat exhibit a jump at the transition temperature  $kT_{t2}/J$ . As the temperature increases, the sublattice order parameters coincide each other at  $kT_{C1}/J$  and this caused the ferromagnetic ordering. At a high temperature above  $kT_{C1}/J$ , the sublattice order parameters  $m_\alpha$  decrease to the value ( $m_\alpha = 0$ ) of  $P$  ordering near the critical temperature  $kT_{C2}/J$ . In the  $F - P$  phase transition, the sublattice susceptibilities and the lattice specific heat has a characteristic peak at  $kT_{C2}/J$ .

In the interval  $-24 < d < -16$ , the model has the  $AB_3(f)$  ground state ordering and shows the successive  $AB_3(f) - F - P$  phase transitions through the  $k = -3$  line. For a selected  $d = -20$  value, the temperature variation of the thermodynamic quantities are illustrated in Fig. 9. In the  $AB_3(f)$  ordering structure, three of the sublattices are occupied by  $B$  ( $S_i = +1$  or  $-1$ ) species ( $m_b = m_c = m_d = 1$ ,  $q_b = q_c = q_d = 1$ ), while the other sublattice is occupied by  $A$  ( $S_i = 0$ ) species ( $m_a = 0$ ,  $q_a = 0$ ). As the temperature increases,  $m_b = m_c = m_d$  and  $q_b = q_c = q_d$  decreases sharply from unity to a value ( $\sim 0.7$ ) of the  $F$  ordering and coincide with  $m_a$  and  $q_a$

at a transition temperature  $kT_t/J$ . However, the model exhibit the second order  $F - P$  phase transition at a critical temperature  $kT_C/J$  above the  $kT_t/J$ . For the  $d = -20$  value  $AB_3(f) - F$  and the  $F - P$  phase transitions are of the first and the second order, respectively. Except the  $d = -20$  value, the  $AB_3(f) - F$  phase transition is of the second order in the interval  $-24 < d < -16$ .

## 2.2. The phase diagrams

The critical behavior of the BEG model near the phase boundaries is investigated using CA algorithm through the  $k = -3$  and  $d = -4$  lines. For  $k = -3$ , the estimated  $(kT_C/J, d)$  phase diagram is shown in Fig. 10. As it is seen in Fig. 1, in the interval  $-24 \leq d < 0$ , the model demonstrates ferromagnetic ( $F$ ), quadrupolar ( $Q$ ) and staggered quadrupolar ( $SQ$ ) ordering regions compatible with the ground state phase diagram on the  $(k, d)$  plane through the  $k = -3$  line. For  $k = -3$ , there are the different types of successive phase transitions as  $AB_3(f) - F - P$ , the  $AB$  (type-I)  $-F - AB$  (type-II)  $-F - P$ , the  $AB$  (type-I)  $-F - P$ , the  $A_3B(a) - A_3B(f) - F - P$  and the  $A_3B(a) - P$ . For all parameter values, the  $F - P$  phase transitions are of the second order. Thus, the paramagnetic  $P$  and the ferromagnetic  $F$  regions are separated with the second order critical line. This behavior is in compatible with the results of the other calculations [28 – 36]. On the other hand, the phase transitions from  $SQ$  orderings to  $F$  and  $P$  orderings are usually of the second order except for a few parameter values. The  $SQ$  ordering and other orderings are separated with second order critical line according to MFA results and CVM results [14, 21, 26], but this critical line is

of the first order according to CVM results [24] for  $k = -3$ . The CA results show that the line between the  $SQ$  and other orderings is not completely a second order critical line, because the model exhibits first order phase transitions for a few parameter value at the critical line. Consequently, our results roughly agree with the MFA ones for type of the critical lines. However, the previous works indicated that the  $SQ$  region generally separated a few of the sub-ordering regions as the ferrimagnetic, the antiquadrupolar and the dense ferromagnetic [14, 24, 26]. For the fcc lattice, there are the Cu-Au ( $A_3B(a)$ ,  $A_3B(f)$ ,  $AB(f)$  and  $AB_3(f)$ ) type orderings [24] in the  $SQ$  region of the phase diagram. However, the Cu-Au type systems exhibit also the  $AB$ (type-II) ordering according to the experimental results [39, 41 – 47] and the theoretical studies [31, 36, 37]. Our calculations demonstrate that the model has the  $AB$  (type-II) ordering regions in addition to  $A_3B(a)$ ,  $A_3B(f)$ ,  $AB(f)$  and  $AB_3(f)$  ordering regions. It is seen from the  $(kT_C/J, d)$  phase diagram that there is the  $A_3B(a)$  ordering in the interval  $-8 < d < 0$ , the  $AB$ (type-I) ordering in the interval  $-16 < d < -8$  and the  $AB_3(f)$  ordering in the interval  $-24 < d < -16$ , at  $kT/J = 0$ . However, in high temperatures, there arise the  $A_3B(f)$  ordering region between the  $AB$ (type-I) and  $AB_3(f)$  ordering regions and  $AB$ (type-II) ordering regions over the  $AB$ (type-I) ordering region. At the phase boundary, the successive  $AB$  (type-I)– $F$  –  $AB$  (type-I)– $F$  –  $AB$  (type-II)– $F$  –  $P$  phase transitions occur between the  $AB$  (type-I) and the  $AB_3(f)$  ground state regions at  $d = -15.9$ . The low temperature phase transitions at this parameter are of the first order. As a result of these phase transitions, two ground state orderings separate with

the first order phase transition line. The phase diagram near this parameter has a cavity including ferromagnetic  $F$  ordering. As a result, the  $SQ$  region splits  $A_3B(a)$ ,  $A_3B(f)$ ,  $AB(\text{type-I})$ ,  $AB(\text{type-II})$  and  $AB_3(f)$  orderings in the different intervals of the  $d$  and the temperature values. The critical temperatures of  $AB(\text{type-I})-F - AB(\text{type-II})$  phase transitions shown as a band (thick line) because of being close each other on the phase diagram.

The  $(kT_C/J, k)$  phase diagram through the  $d = -4$  line is presented in Fig. 11. Through the  $d = -4$  line, our calculations indicate that, there are the  $AB_3(f)$  ordering in the interval  $-15 < k < -1.35$ , the  $AB(\text{type-I})$  ordering in the interval  $-2 < k < -1.5$  and the  $A_3B(a)$  ordering for  $k < -2$  at  $kT/J = 0$ . The  $(kT_C/J, k)$  phase diagram for  $d = -4$  does not have the  $A_3B(f)$  ordering which occur between  $AB(\text{type-I})$  and  $A_3B(a)$  regions through the  $k = -3$  line. It indicates that the  $A_3B(f)$  ordering region becomes narrow with increasing  $k$  value on the  $SQ$  ordering region of the  $(k, d)$  plane. In the interval  $-2 < d < -1.5$  above the  $AB(\text{type-I})$  ordering, there occur  $AB(\text{type-II})$  ordering regions for the certain parameter regions as the  $(kT_C/J, d)$  phase diagram for  $k = -3$ . The  $AB(\text{type-II})$  ordering vanishes near the  $A_3B(P)$  ground state ordering region in the interval  $-2 < k \leq -1.75$ . For the different  $k$  values through the  $d = -4$  line, the model exhibits the  $AB(\text{type-I})-F - AB(\text{type-II})-F - P$ , the  $AB(\text{type-I})-F - P$ , the  $A_3B(a)-F - P$  and the  $AB_3(f) - F$  type successive phase transitions. In this phase transition, the  $A_3B(a)-F$ , the  $A_3B(a)-P$ , the  $AB(\text{type-I})-F$  phase transition at  $k = -1.8$  value and the  $AB_3(f)-F$  phase transitions in the  $-1.41 < k \leq -1.35$  parameter region are of the first order while the

other transitions are of the second order. Consequently, the CA results for the  $(kT_C/J, d)$  and the  $(kT_C/J, k)$  phase diagrams through the  $k = -3$  and  $d = -4$  lines show that the model has the  $A_3B$ ,  $AB$  and  $AB_3$  ground state ordering regions on the  $(k, d)$  plane which is illustrated in Fig. 1. However, there are different type critical behaviors in the phase boundaries between these regions and new ordering structures in the high temperature region over the ground state.

### 3. Conclusion

The spin-1 Ising BEG model has been simulated using the heating algorithm of the cellular automaton for the face-centered cubic lattice. The simulations show that the BEG model has the Cu-Au type stoichiometric  $A_3B(a)$ ,  $A_3B(f)$ ,  $AB(\text{type-I})$ ,  $AB(\text{type-II})$  and  $AB_3(f)$  orderings in the staggered quadrupolar region for  $k < -1$ . Furthermore, the  $A_3B(a)$ ,  $A_3B(f)$ ,  $AB(\text{type-I})$  and  $AB_3(f)$  ordering regions exhibit the different successive phase transitions. The phase diagrams on the  $(kT_C/J, d)$  and the  $(kT_C/J, k)$  planes are obtained for  $k = -3$  and  $d = -4$ , respectively. The cellular automaton (CA) results reconstruct the phase boundaries on the  $(kT_C/J, d)$  phase diagrams which indicated by the other calculations [14, 24, 26]. It is seen that the model exhibits the successive and the multi phase transitions from the first or the second order near the phase boundaries. The  $SQ$  ordering and the other orderings are separated with the second order critical line according to MFA results [14], but this critical line is of the first order according to CVM results [24] for  $k = -3$ . The CA results roughly agree with the MFA ones for type of the critical lines. In addition, it is seen that the fcc BEG model

has the modulated  $AB$  (type-II) phase as indicated by the experimental results [39, 41 – 47]. The modulated  $AB$  (type-II) phase is obtained above the  $AB$  (type-I) phase which was indicated by the CVM [24] on the  $(kT_C/J, d)$  plane. Furthermore, the heating rate is effective for separating the phase transitions which are close. The obtained results show that the BEG model is very suitable for studying with the binary alloys. Furthermore, the heating algorithm improved from Creutz cellular automaton is successful for exposing the critical behavior of the BEG model.

### Acknowledgement

This work is supported by a grant from Gazi University (BAP:05/2003-07).

1. M. Blume, V.J. Emery and R.B.Griffiths, *Phys. Rev. A* 4, 1071 (1971).
2. J. Lajzerowicz and J. Siverdière, *Phys. Rev. A* 11, 2079 (1975).
3. J. Lajzerowicz and J. Siverdière, *Phys. Rev. A* 11, 2090 (1975); J. Lajzerowicz and J. Siverdière, *Phys. Rev. A* 11, 2101 (1975).
4. M. Schick and W.H. Shih, *Phys.Rev. B* 34, 1797 (1986).
5. R. Osório, S. Froyen, *Phys. Rev. B* 47, 1889 (1993).
6. B.L. Gu, K.E. Newman, P.A. Fedders, *Phys. Rev. B* 35, 9135 (1987).
7. Z.X. Cai, S.D. Mahanti, *Phys. Rev. B* 36, 6928 (1987).
8. M. Ausloos, P. Clippe, J.M. Kowalski, A. Pekalski, *Phys. Rev. A* 22, 2218 (1980).
9. M. Ausloos, P. Clippe, J.M. Kowalski, J. Pekalska, A. Pekalski, *Phys. Rev. A* 28, 3080 (1983).
10. M. Droz, M. Ausloos, J.D. Gunton, *Phys. Rev. B* 18, 388 (1978).

11. M. Ausloos, P. Clippe, J.M. Kowalski, A. Pekalski, *IEEE Trans. Magnetica MAG* 16, 233 (1980).
12. M. Ausloos, P. Clippe, J.M. Kowalski, J.P. Ekalska, A. Pekalski, *J. magnet. and magnet. matter* 39, 21 (1983).
13. H.H. Lee, D.P. Landau, *Phys. Rev. B* 20, 2893 (1979).
14. W. Hoston and A.N. Berker, *Phys. Rev. Lett.* 67, 1027 (1991).
15. N. Seferoğlu and B. Kutlu, *Physica A* 374, 165 (2007).
16. A.Özkan, B.Kutlu, *Int.J.of Mod.Phys C* 18, 1417 (2007).
17. K.E. Newman and J.D. Dow, *Phys. Rev. B* 27, 7495 (1983).
- 18 M. Kessler, W. Dieterich and A. Majhofer, *Phys. Rev. B* 67,134201 (2003).
19. H. Ez-Zahraouy, L. Bahmad, A. Benyoussef, *Brazillian J. of Phys.* 36, 557 (2006).
20. R.R. Netz, A.N. Berker, *Phys. Rev.B* 47, 15019 (1993).
21. W. Hoston and A.N. Berker, *J. App. Phys.* 70, 6101 (1991).
22. K. Kasono, I Ono, *Z.Phys. B: Condens. Matter* 88, 205 (1992).
23. Y.L. Wang, F. Lee, J.D. Kimel, *Phys. Rev. B* 36, 8945 (1987).
24. S. Lapinskas and A. Rosengren, *Phys. Rev. B* 49, 15190 (1994).
25. P.J. Kundrotas, S. Lapinskas and A. Rosengren, *Phys. Rev. B* 56, 6486 (1997).
26. C. Ekiz and M. Keskin, *Phys. Rev. B* 66, 054105 (2002).
27. R.R. Netz, *Europhys. Lett.* 17, 373 (1992).
28. M.K. Phani, J.L. Lebowitz, M.H. Kalos, C.C. Tsai, *Phys. Rev. Lett.* 42, 577 (1979).

29. K. Binder, *Phys. Rev. Lett.* 45, 811 (1980).
30. D.F. Styer, M.K. Phani, J.L. Lebowitz, *Phys. Rev.B* 34, 3361 (1986).
31. Z. Xi, B. Chakraborty, K.W. Jacobsen, J.K. Norskov, *J.Phys:Cond. Matt.* 4, 7191 (1992).
32. G. Bozzolo, B. Good, J. Ferrante, *NASA Technical Memorandum* 107168 (1996).
33. S.H. Wei, A.A. Mbaye, L.G. Ferreira, A. Zunger, *Phys. Rev. B* 36, 4163 (1987).
34. J.M. Sanchez, C.H. Lin, *Phys. Rev. B* 30, 1448 (1984).
35. A.D. Beath, D.H. Ryan, *Physical Rev. B* 72, 014455 (2005).
36. B. Chakraborty, Z. Xi, *Phys. Rev. Lett.* 68, 2039 (1992).
37. M. Tachiki, *Phys. Rev.* 150, 440 (1966).
38. L. Barbier, S. Goapper, B. Salanon, R. Caudron, A. Loiseau, J. Alvarez, S. Ferrer, X. Torrelles, *Phys. Rev. Lett.* 78, 3003 (1997).
39. R.G. Jordan, Y. Jiang, M.A. Hoyland, A.M. Begley, *Physical Rev.B* 43, 12173 (1991).
40. I.L. Guhr, B. Riedlinger, M. Maret, U. Mazur, A. Barth, F. Treubel, M. Albrecht, G. Schatz, *J. of Applied Physics* 98, 063520 (2005).
41. E.C. Bain, *Chem. Met. Eng.* 28, 21 (1923).
42. A. Pianelli, R. Faivre, *Compt. Rend.* 245, 1537 (1957).
43. T. Shinohara, S. Saitoh, F. Wagatsuma, S. Yamaguchi, *Philosophical Magazine A* 79, 437 (1999) .
44. R.A. Oriani, *Acta metall.* 2, 608 (1954).
45. F.N. Rhines, W.E. Bond, R.A. Rummel, *Trans. Amer. Soc. Met.* 47,

578 (1955).

46. H. Sato, R.S. Toth, *Phys. Rev.* 124, 1833 (1961).
47. K. Sato, D. Watanabe, S. Ogawa, *J. Pyhs. Soc. Jpn* 17, 1647 (1962).
48. B. Kutlu, *Int. J. Mod. Phys. C* 14, 1401 (2001).
49. B. Kutlu, *Int. J. Mod. Phys. C* 14, 1305 (2003).
50. B. Kutlu, A. Özkan, N. Seferoğlu, A. Solak and B. Binal, *Int. J. Mod. Phys.C* 16, 933 (2005).
51. A. Özkan, N. Seferoğlu and B. Kutlu, *Physica A* 362, 327 (2006).
52. N. Seferoğlu and A. Özkan and B. Kutlu, *Chin. Phys. Lett.* 23, 2526 (2006).
53. M. Creutz, *Phys. Rev. Lett.* 50, 1411 (1983).
54. B. Kutlu, N. Aktekin, *J. Stat.Phys.* 75, 757 (1994).
55. B. Kutlu, N. Aktekin, *Physica A* 215, 370 (1995).
56. B. Kutlu, *Physica A* 234, 807 (1997).
57. B. Kutlu, *Physica A* 243, 199 (1997).
58. N. Aktekin, *Annual Reviews of computational physics VII* , ed. D.Stauffer (World Scientific, Singapore, 2000) p. 1.
59. C. Dress, *J.of physics A* 28, 7051 (1995).
60. K. Saito, S. Takesue and S. Miyashita, *Phys.Rev.E* 59, 2783 (1999).
61. T.M. Gwizdella, *Czechoslovak J. of Phys.* 54, 679 (2004).
62. Z. Merdan, M. Bayırlı, *Applied Mathematics and Computation* 167, 212 (2005).
63. T.M. Gwizdella, *Phys. Lett. B* 19, 169 (2005).
64. Z. Merdan, D. Atille, *Physica A* 376, 327 (2007).

65. N. Aktekin, S. Erkoç, *Physica A* 290, 123 (2001).
66. N. Aktekin, S. Erkoç, *Physica A* 284, 206 (2000).
67. Z. Merdan, R. Erdem, *Phys. Lett. A* 330, 403 (2004).
68. A.T.Paxton, H.M.Polatoglou, *Phys. Rev. Lett.* 78, 270 (1997).
69. A.Yamamoto, *Acta Cryst.* 38, 1446 (1982).
70. B.Chakraborty, *Phys. Rev. B* 49, 8608 (1994).

### Figure Captions

Fig. 1. The ground state phase diagram ( $k, d$ ) of the BEG model on the fcc lattice.

Fig. 2. The four sublattices for an fcc lattice. The circle, the square, the diamond and the triangle indicate the  $m_a$ ,  $m_b$ ,  $m_c$  and  $m_d$  sublattices, respectively.

Fig. 3. For  $d = -4$ , the temperature dependence of (a) the lattice order parameters ( $M, Q$ ) and sublattice order parameters ( $m_\alpha, q_\alpha$ ), (b) the sublattice susceptibility ( $\chi_a$ ), (c) the lattice Ising energy ( $H_I$ ), and (d) the lattice specific heat ( $C/k$ ) at  $k = -3$  on  $L=9$ .

Fig. 4. For  $d = -7$ , the temperature dependence of (a) the sublattice order parameters ( $m_\alpha, q_\alpha$ ), (b) the lattice susceptibility ( $\chi$ ) and the sublattice susceptibility ( $\chi_a$ ), (c) the lattice Ising energy ( $H_I$ ), and (d) the lattice specific heat ( $C/k$ ) at  $k = -3$  on  $L=9$ .

Fig. 5. For  $d = -7.7$ , the temperature dependence of (a) the sublattice order parameters ( $m_\alpha, q_\alpha$ ), (b) the sublattice susceptibility ( $\chi_a$ ), (c) the lattice Ising energy ( $H_I$ ) and (d) the lattice specific heat ( $C/k$ ) at  $k = -3$  on  $L=9$ .

Fig. 6. For  $d = -12$ , the temperature dependence of (a) the sublattice order parameters  $(m_\alpha, q_\alpha)$ , (b) the sublattice susceptibility  $(\chi_a)$ , (c) the lattice Ising energy  $(H_I)$  and (d) the lattice specific heat  $(C/k)$  at  $k = -3$  on  $L=9$ .

Fig. 7. For  $d = -14.5$ , the temperature dependence of (a) the sublattice order parameters  $(m_\alpha, q_\alpha)$ , (b) the sublattice susceptibility  $(\chi_a)$ , (c) the lattice Ising energy  $(H_I)$  and (d) the lattice specific heat  $(C/k)$  on  $L=9$  at  $k = -3$ .

Fig. 8. For  $d = -15.8$ , the temperature dependence of (a) the sublattice order parameters  $(m_\alpha, q_\alpha)$ , (b) the sublattice susceptibility  $(\chi_a)$ , (c) the lattice Ising energy  $(H_I)$  and (d) the lattice specific heat  $(C/k)$  at  $k = -3$  on  $L=9$ .

Fig. 9. For  $d = -20$ , the temperature dependence of (a) the sublattice order parameters  $(m_\alpha, q_\alpha)$ , (b) the sublattice susceptibility  $(\chi_a)$ , (c) the lattice Ising energy  $(H_I)$  and (d) the lattice specific heat  $(C/k)$  at  $k = -3$  on  $L=9$ .

Fig. 10. The phase diagram in the  $(kT_C/zJ, d)$  plane for  $k = -3$  on  $L=9$ . The closed and open symbols indicate the second and the first order phase transitions, respectively. The thick line indicates the ferromagnetic ( $F$ ) ordering.

Fig. 11. The phase diagram in the  $(kT_C/zJ, k)$  plane for  $d = -4$  on  $L=9$ . The closed and open symbols indicate the second and the first order phase transitions, respectively. The thick line indicates the ferromagnetic ( $F$ ) ordering.

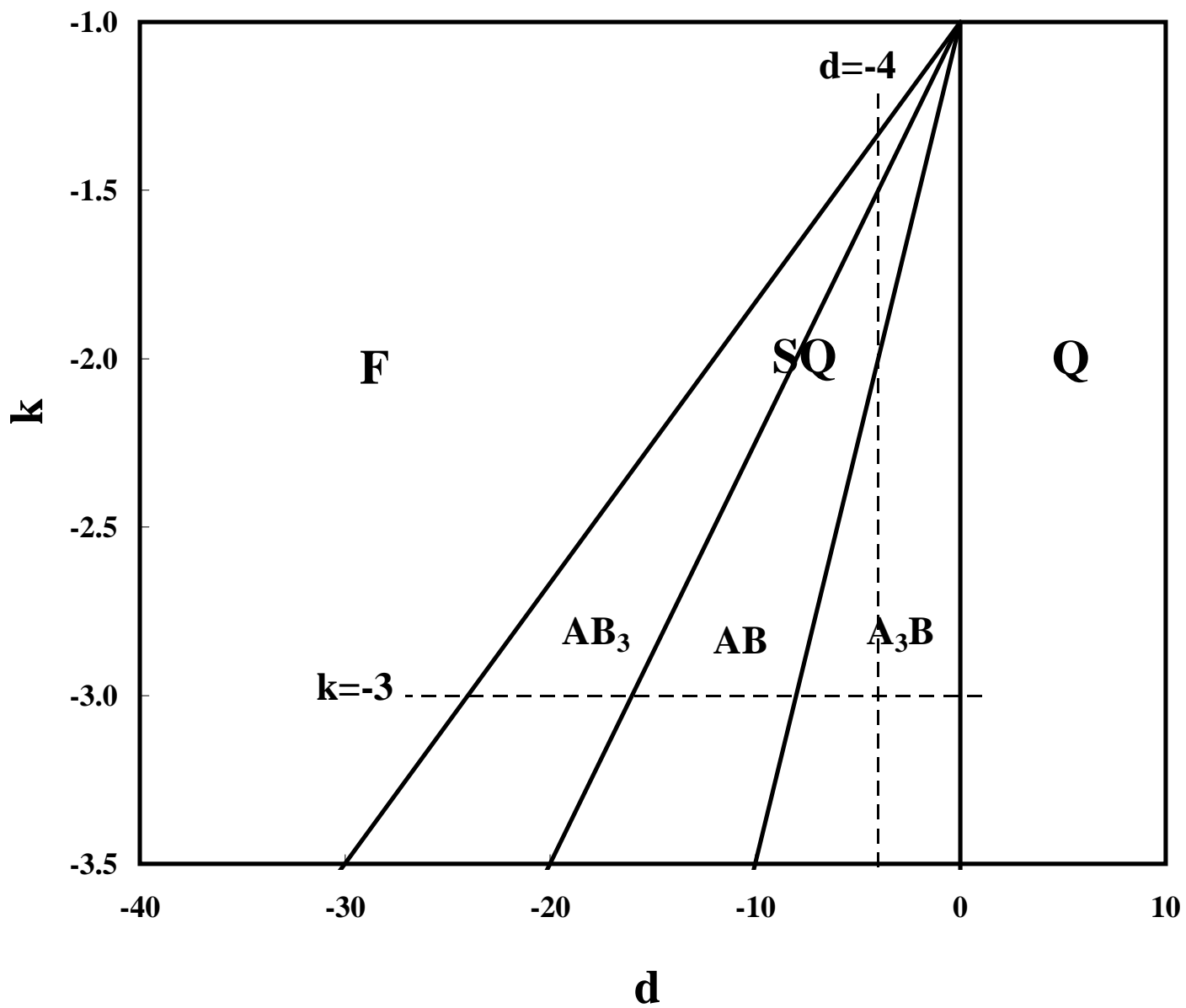


Figure 1

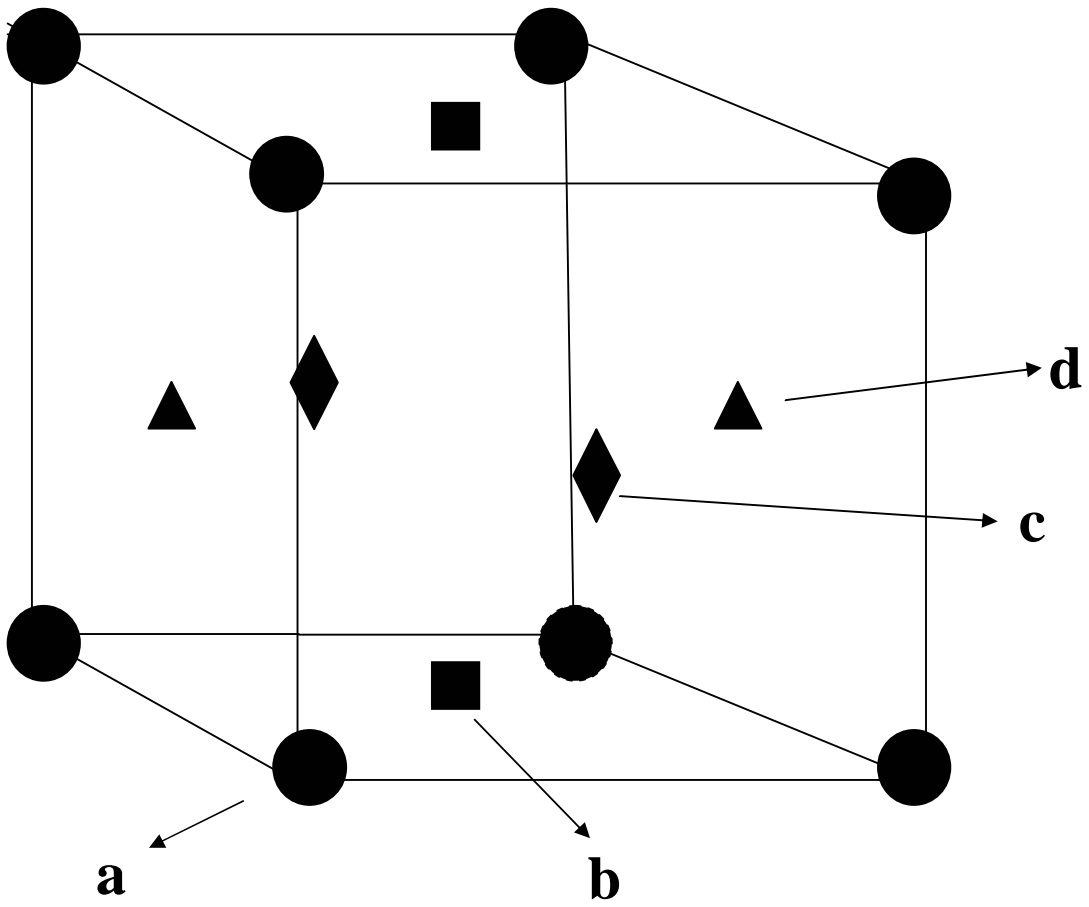


Figure 2

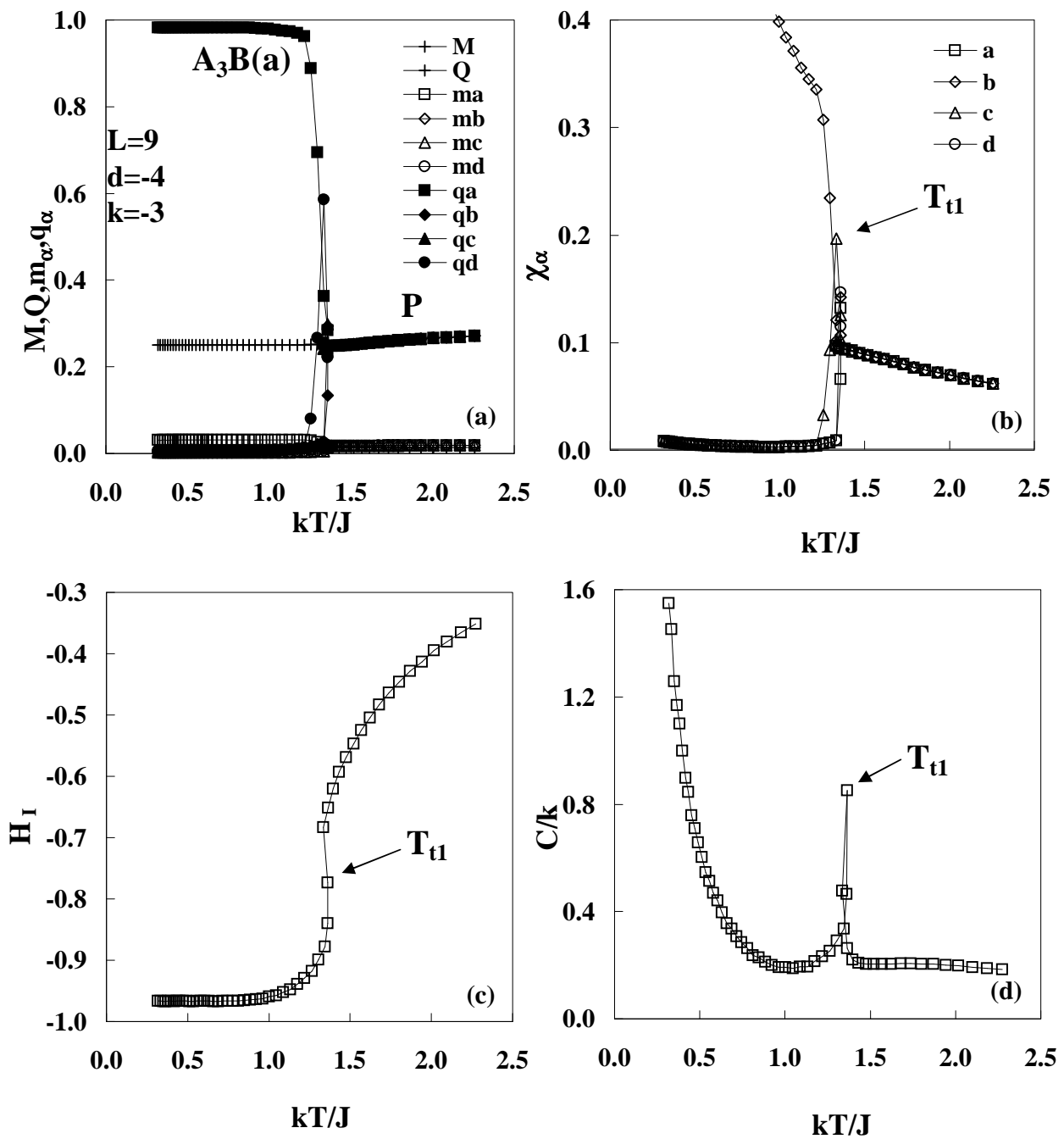


Figure 3

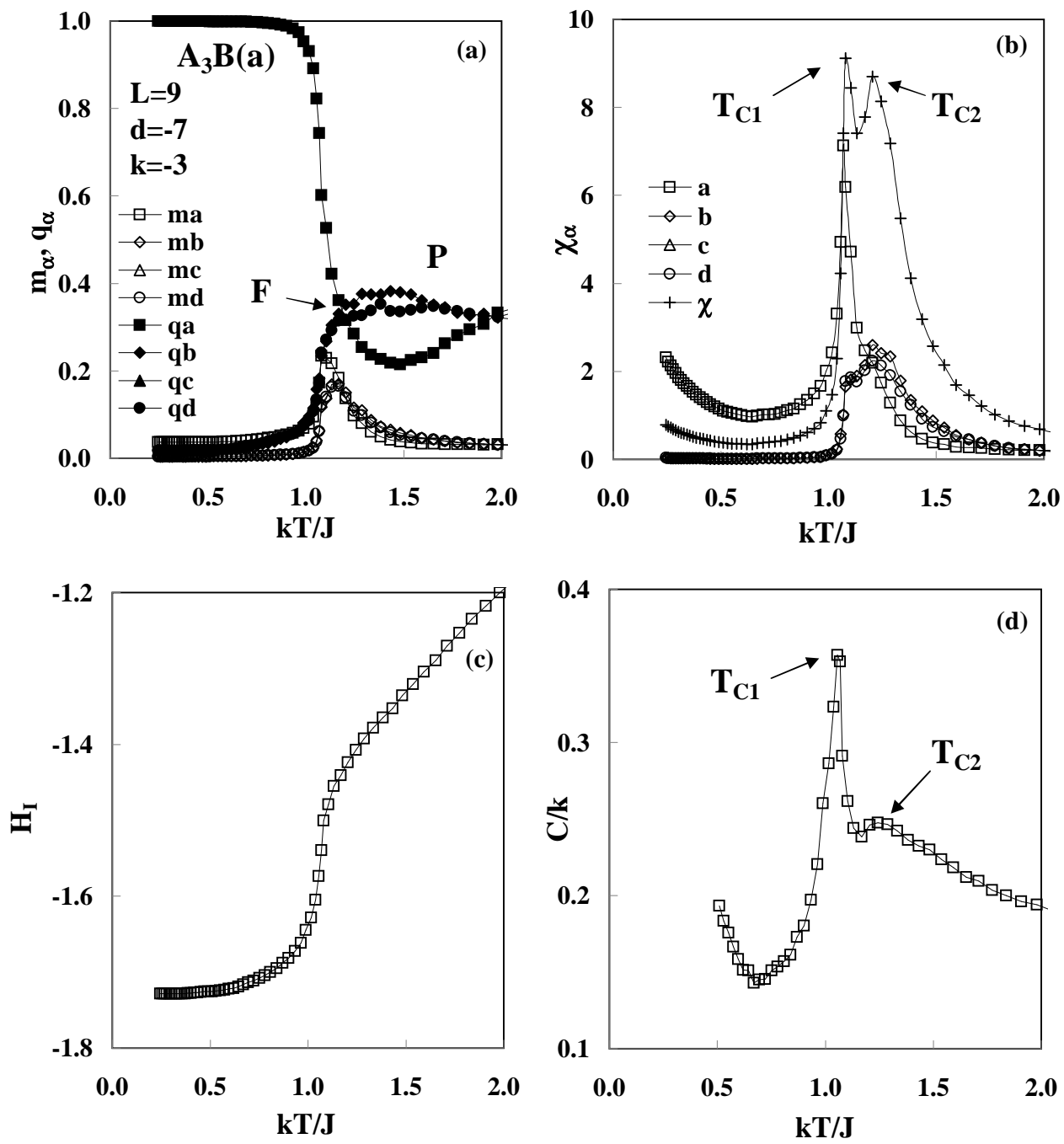


Figure 4

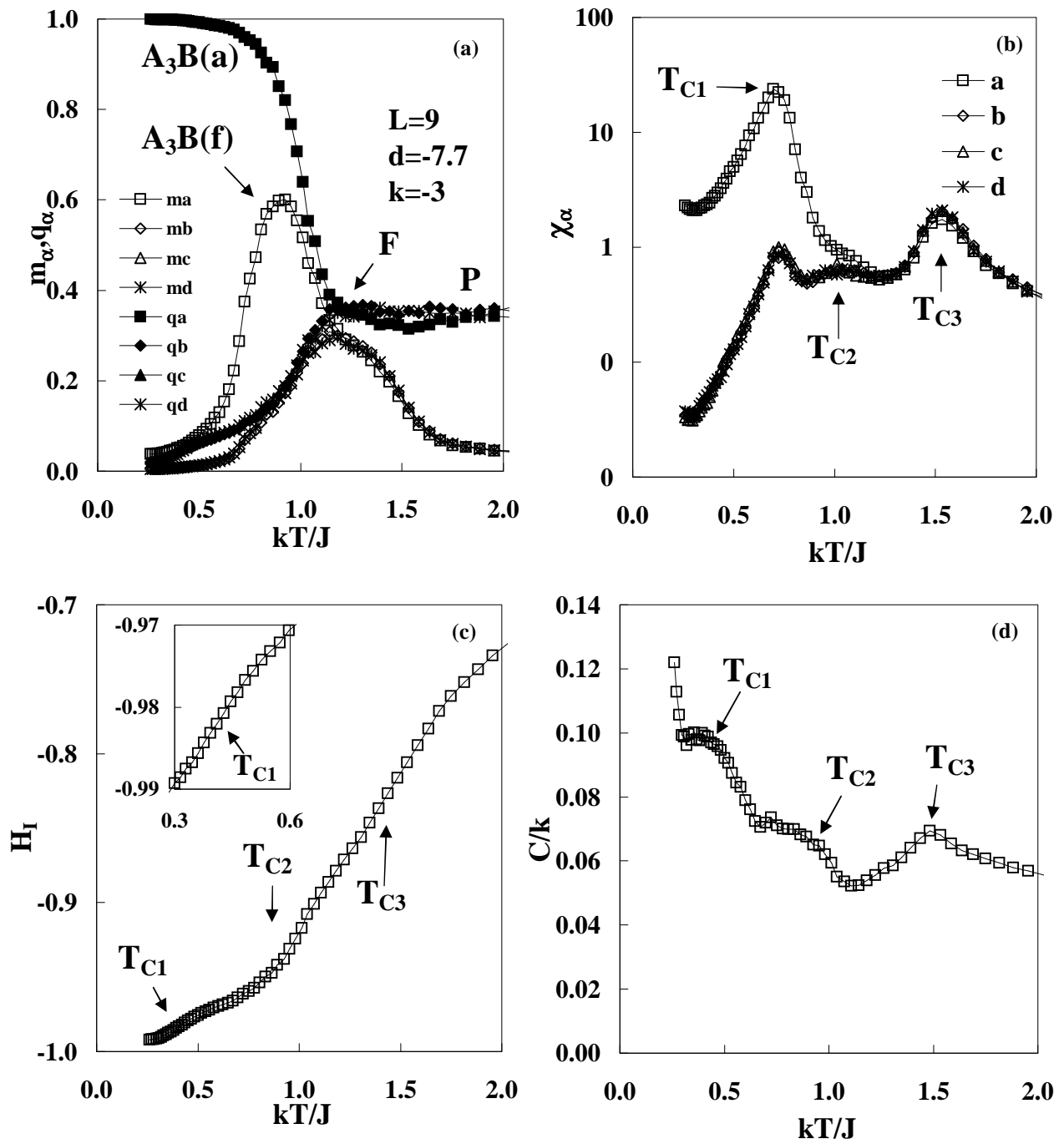


Figure 5

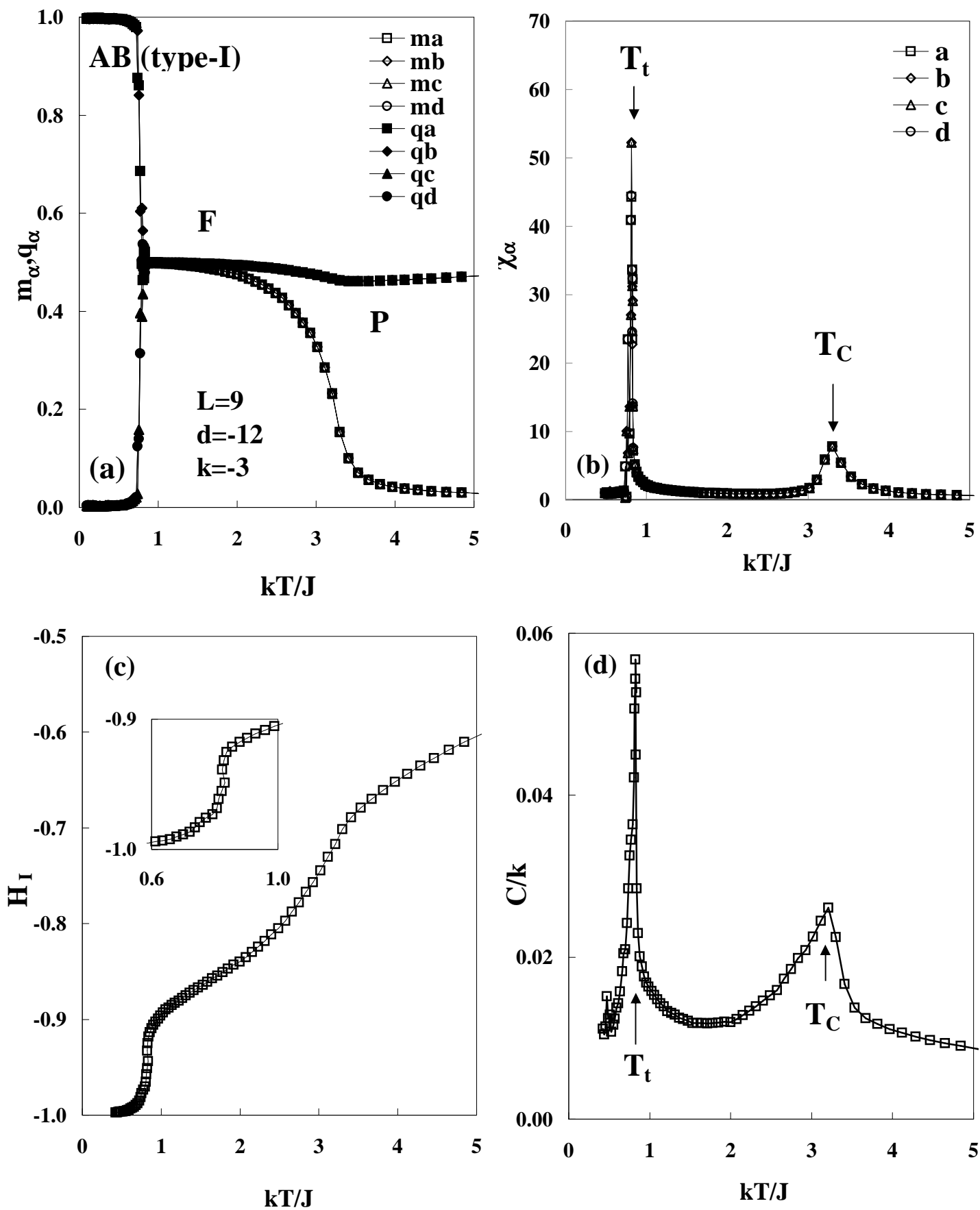


Figure 6

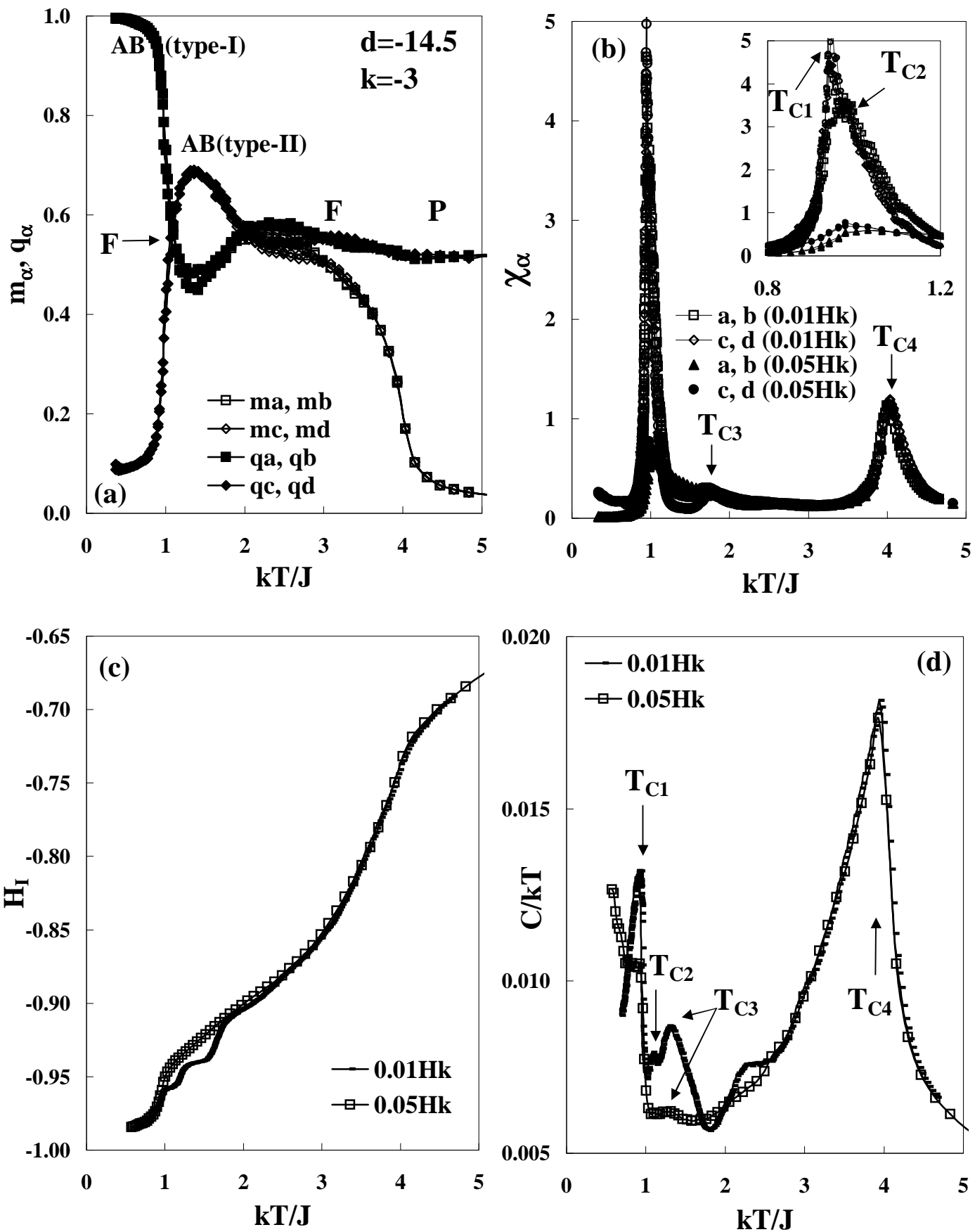


Figure 7

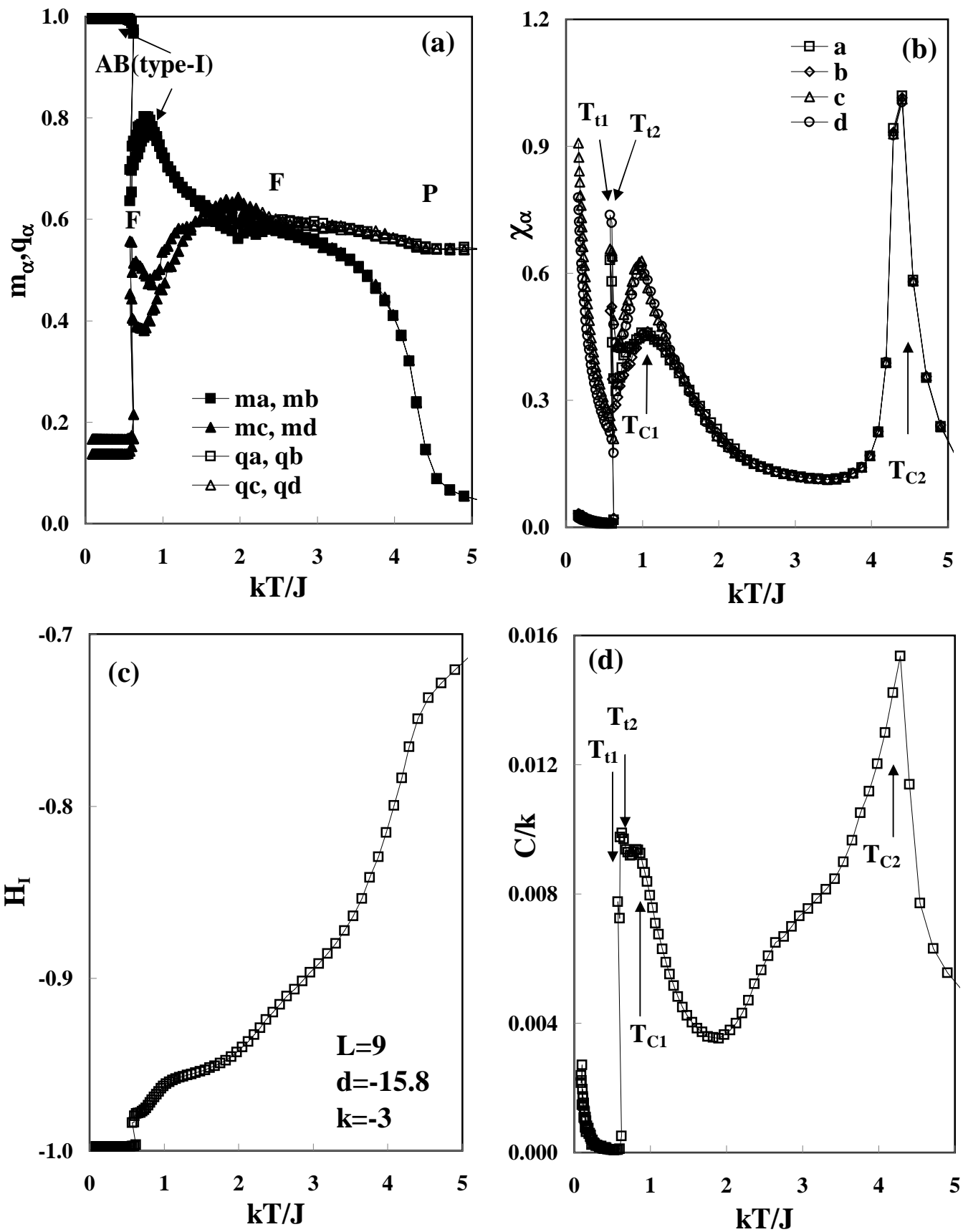


Figure 8

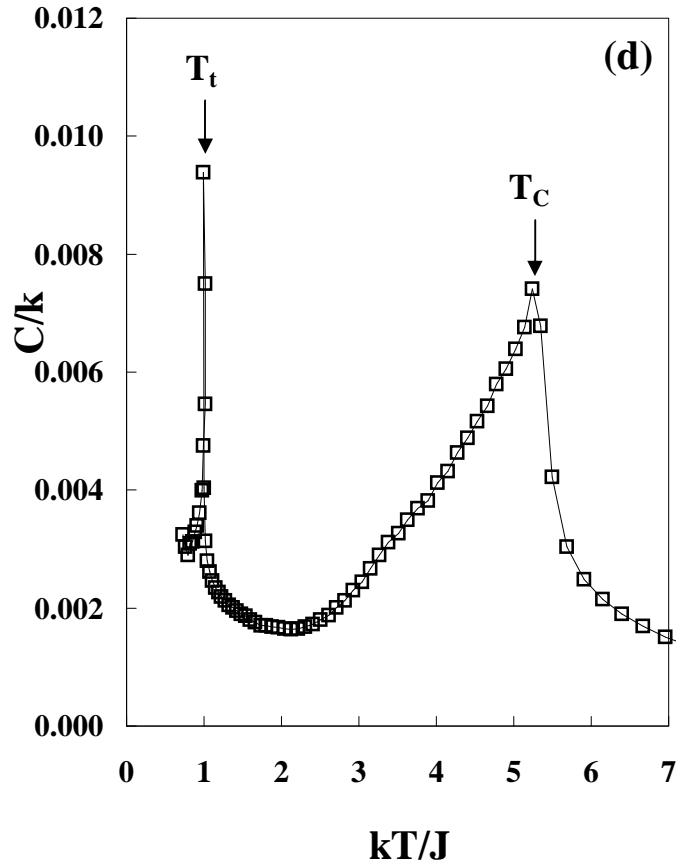
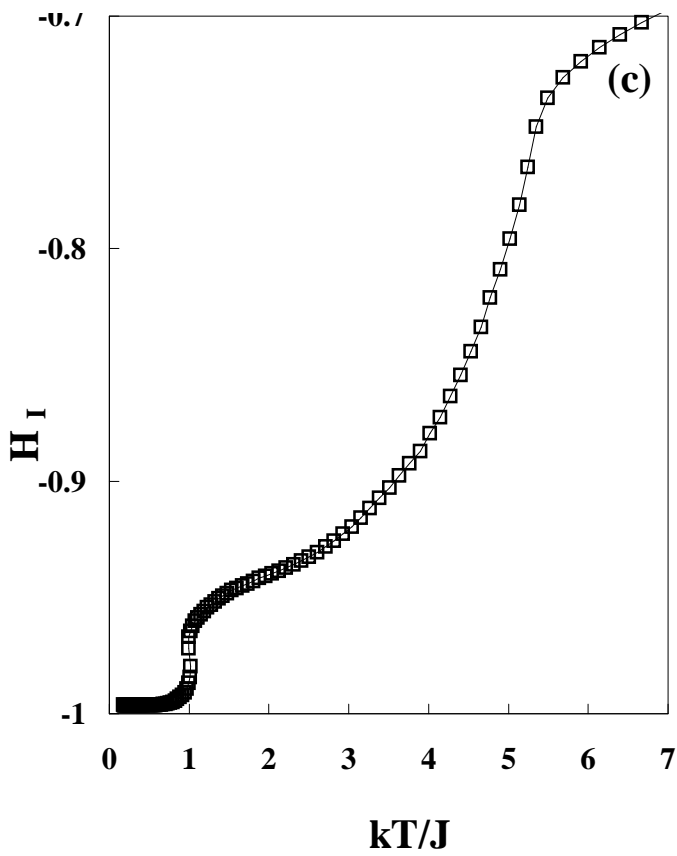
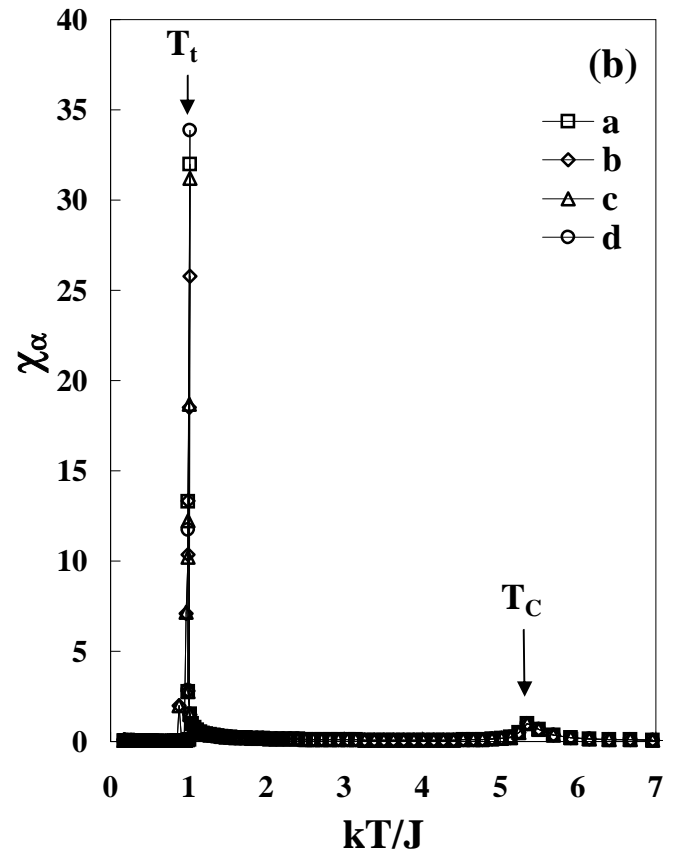
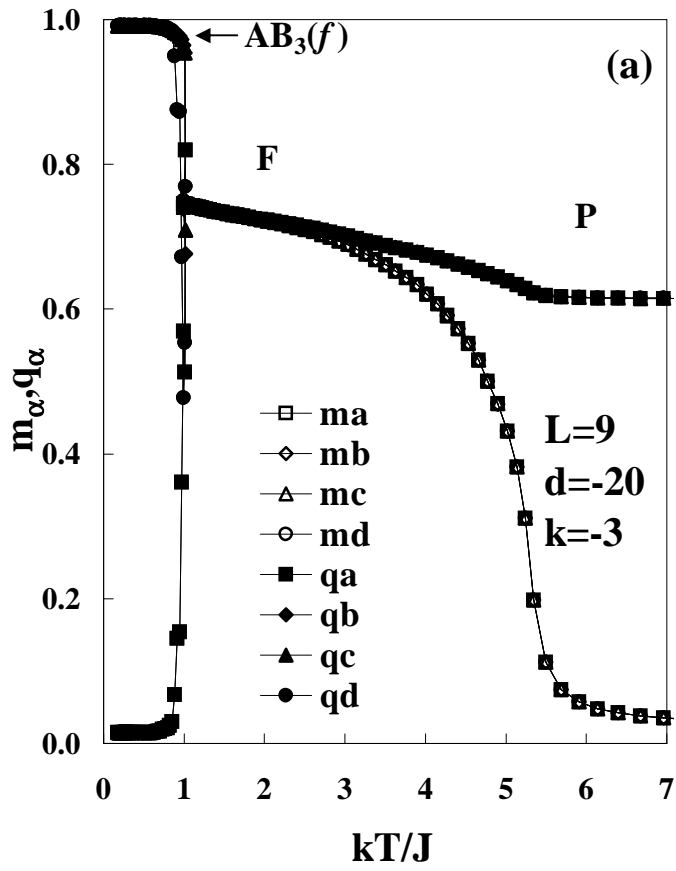


Figure 9

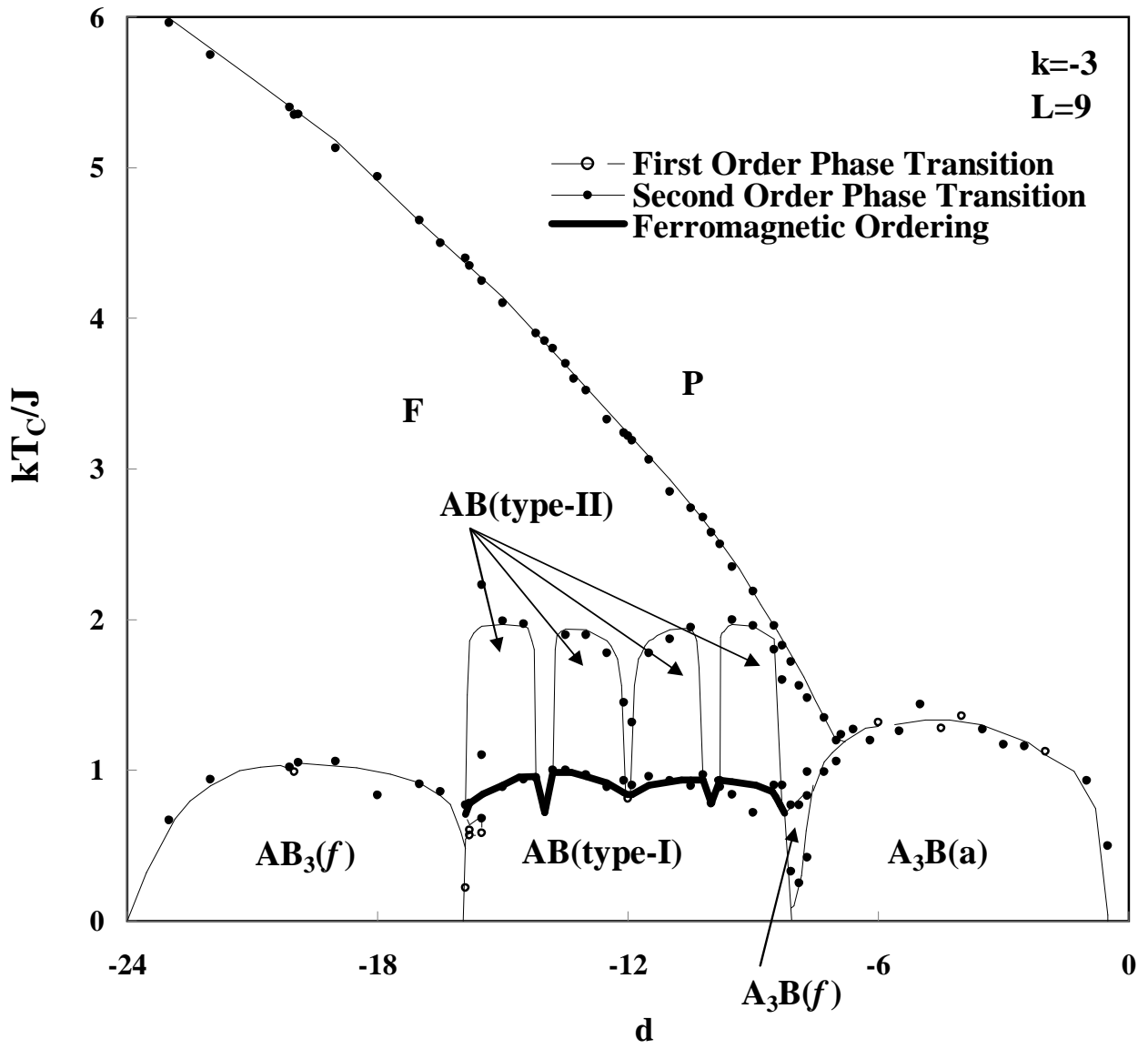


Figure 10

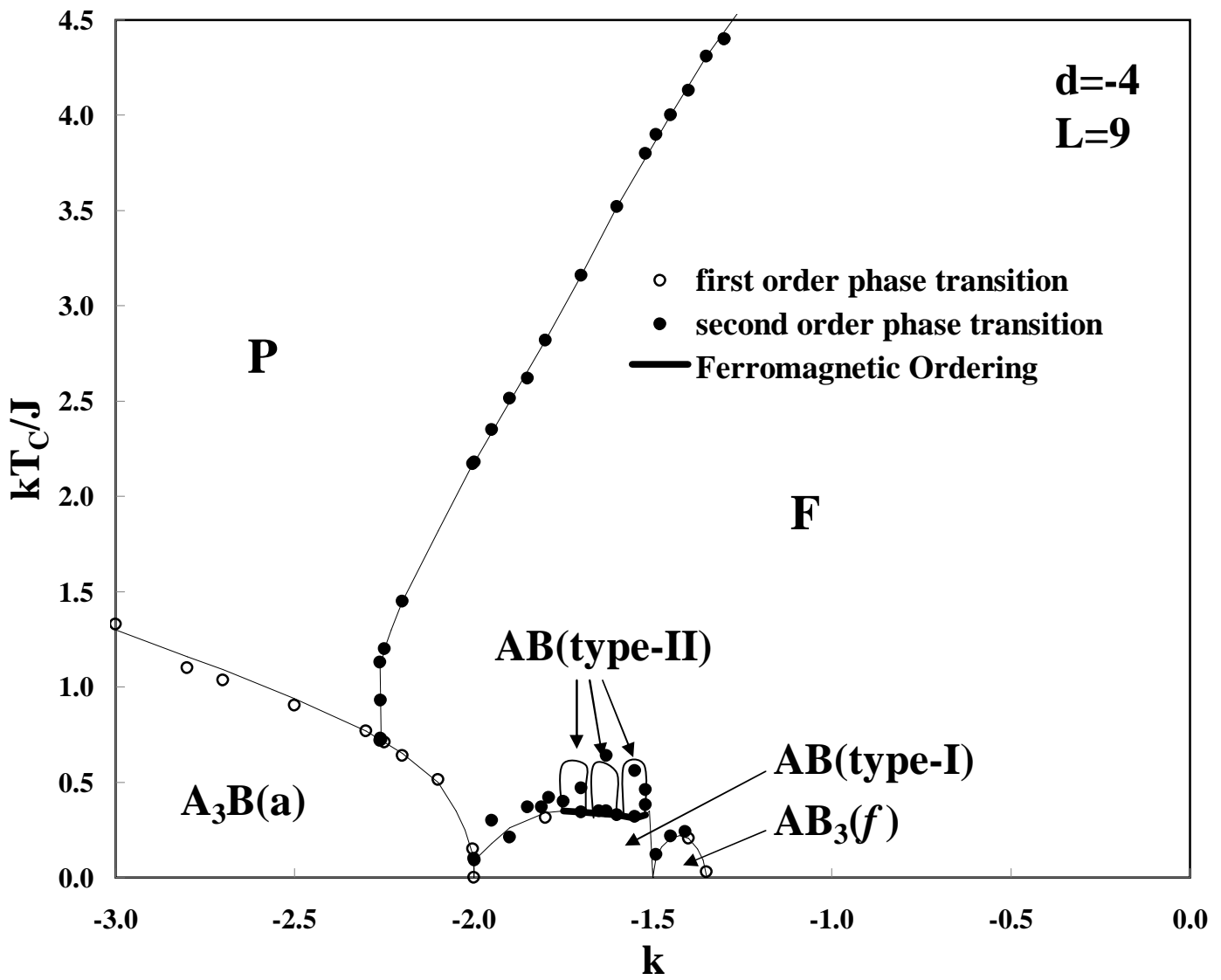


Figure 11